International Journal of Thermophysics, Vol. 19, No. 5, 1998

Molar Heat Capacity at Constant Volume of 1,1-Difluoroethane (R152a) and 1,1,1-Trifluoroethane (R143a) from the Triple-Point Temperature to 345 K at Pressures to 35 MPa

J. W. Magee[1]

Received October 31, 1997

Molar heat capacities at constant volume (C_v) of 1,1-difluoroethane (R152a) and 1,1,1-trifluoroethane (R143a) have been measured with an adiabatic calorimeter. Temperatures ranged from their triple points to 345 K, and pressures up to 35 MPa. Measurements were conducted on the liquid in equilibrium with its vapor and on compressed liquid samples. The samples were of high purity, verified by chemical analysis of each fluid. For the samples, calorimetric results were obtained for two-phase ($C_v^{(2)}$), saturated-liquid (C_σ or C_x'), and single-phase (C_v) molar heat capacities. The C_σ data were used to estimate vapor pressures for values less than 105 kPa by applying a thermodynamic relationship between the saturated liquid heat capacity and the temperature derivatives of the vapor pressure. The triple-point temperature and the enthalpy of fusion were also measured for each substance. The principal sources of uncertainty are the temperature rise measurement and the change-of-volume work adjustment. The expanded relative uncertainty (with a coverage factor $k = 2$ and thus a two-standard deviation estimate) for C_v is estimated to be 0.7%, for $C_v^{(2)}$ it is 0.5%, and for C_σ it is 0.7%.

KEY WORDS: 1,1-difluoroethane; enthalpy of fusion; heat capacity; 1,1,1-trifluoroethane; triple point; R143a; R152a; vapor pressure.

1. INTRODUCTION

Thermodynamic properties of a fluid may be calculated from a knowledge of its ideal-gas properties and an accurate equation of state. Heat capacities

[1] Physical and Chemical Properties Division, Chemical Science and Technology Laboratory, National Institute of Standards and Technology, Boulder, Colorado 80303, U.S.A.

0195-928X/98/0900-1397$15.00/0

derived in this manner, however, often lack sufficient accuracy since the calculation involves integration of isochoric curvature $(\partial^2 p/\partial T^2)_\rho$ as in the equation:

$$C_v - C_v^\circ = -T \int_0^\rho \left(\frac{\partial^2 p}{\partial T^2}\right)_\rho \frac{d\rho}{\rho^2} \tag{1}$$

where C_v° is the ideal-gas heat capacity. The quantity $(\partial^2 p/\partial T^2)_\rho$ is known to possess small absolute values, except in the vicinity of the critical point, and is very difficult to measure accurately. In the case of compressed liquid states, additional data are required, including the vapor pressure and enthalpy of vaporization or heat capacity of the saturated liquid. Direct measurements of heat capacities provide useful checks on calculated heat capacities when they are available along a path traversing the temperature range of interest. Unfortunately, such data are often scarce. Only three other publications of heat capacity data for R152a and only one publication (with 11 data points) for R143a are now available.

In this paper, heat capacity data are reported for both the single-phase liquid and the saturated liquid region from near the triple-point temperature to the upper limit (345 K) of the apparatus. In addition, vapor pressures evaluated from the saturated-liquid heat capacity data and measurements of the enthalply of fusion and triple-point temperature for each substance are reported.

2. MEASUREMENTS

2.1. Apparatus and Procedures

The calorimeter used for these measurements has been described in detail by Goodwin [1] and Magee [2]. A spherical bomb contains a sample of known mass. The volume of the bomb, approximately 73 cm^3, is a function of temperature and pressure. A platinum resistance thermometer is attached to the bomb for the temperature measurement. Temperatures are reported on the ITS-90, after conversions from the original calibration on the IPTS-68. Pressures are measured with an oscillating quartz crystal pressure transducer with a 0 to 70 MPa range. Adiabatic conditions are ensured by a high vacuum (3×10^{-3} Pa) in the can surrounding the bomb, by a temperature-controlled radiation shield, and by a temperature-controlled guard ring which thermally anchors the filling capillary and the lead wires to the bomb.

For the heat-capacity measurement, a precisely determined electrical energy (Q) is applied and the resulting temperature rise ($\Delta T = T_2 - T_1$) is measured. We obtain the heat capacity from

$$C_v = \left(\frac{\partial U}{\partial T}\right)_v = \frac{Q - Q_0 - W_{pV}}{n\,\Delta T} \tag{2}$$

where U is the internal energy, Q_0 is the energy required to heat the empty calorimeter, W_{pV} is the change-of-volume work that results from the slight dilation of the bomb, and n is the number of moles enclosed in the bomb. In this work, the bomb was charged with sample up to the (p, T) conditions of the highest-density isochore. The bomb and its contents were cooled to a starting temperature in the single-phase liquid region. Then, measurements were performed in that region with increasing temperature until either the upper temperature (345 K) or pressure limit (35 MPa) was attained. The bomb was then cooled to a temperature near the triple point, and measurements were begun in the two-phase region and continued into the single-phase region, up to the same limits. At the completion of a run, a small part of the sample was cryopumped into a lightweight cylinder for weighing. The next run was started with a smaller density. A maximum of four runs was measured with one filling of the bomb. When these runs were completed, the remaining sample was discharged and weighed.

A series of such runs with different fillings constitutes the investigation of the (p, T, C_v) surface. The ranges of temperature and pressure were predetermined to overlap published measurements of heat capacity for R152a and R143a. Within these ranges, C_v measurements were performed on eight isochores for 85 state conditions for R152a at (164 to 342 K, 3.0 to 33.4 MPa) and on seven isochores for 136 state conditions for R143a at (172 to 342 K, 3.1 to 34.3 MPa). The two-phase heat capacity (leading to C_σ) measurements followed the path of (p, T) states defined by the vapor-pressure curves. For R152a, 66 two-phase points were measured at temperatures from 162 to 315 K, and 80 two-phase points were measured for R143a at temperatures from 165 to 341 K. A search of the literature disclosed only three sources of heat capacity measurements at constant pressure (C_p) for R152a and one source for R143a. No published C_v data were found. Kubota et al. [3] reported C_p measurements for R152a at temperatures from 313 to 353 K and at pressures from 0.5 to 1.4 MPa; Nakagawa et al. [4] have reported C_p measurements at temperatures from 276 to 360 K and at pressures from 1 to 3.2 MPa; and Porichanski et al. [5] have reported C_p measurements at temperatures from 220 to 425 K and at pressures from 2 to 20 MPa. Russell et al. [6] have reported C_p

measurements for R143a at temperatures from 165 to 221 K at conditions of the saturated liquid.

2.2. Samples

High-purity samples were obtained for the measurements. The sample of R152a had the highest purity, 0.99962 mass fraction. The largest impurity was $CHClF_2$ (R22) with a mass fraction of 0.00036. Other impurities included 10 ppm of CH_3CClF_2 (R142b), and 10 ppm of C_2H_6O. The purity of the R143a sample was approximately 0.9993 mass fraction. An infrared spectrum and three types of chromatographic analyses were recorded for the sample. A small quantity of an unidentified impurity (0.0007 mass fraction) was detected in two of the three chromatographic analyses. The mass spectrum of the impurity is consistent with a substance of slightly higher molecular mass than R143a, but the pattern was too weak to identify the impurity.

3. RESULTS

3.1. Heat Capacity

As mentioned in Section 2.1, adjustments should be applied to the raw heat-capacity data for the change-of-volume work of the bomb. During a measurement sequence, the volume of the bomb varies with temperature and pressure in accordance with formulas reported previously [2]. It is an important adjustment since the bomb is thin-walled. Referring to Goodwin and Weber [7], we can obtain the work from

$$W_{pV} = \left(T_2 \left(\frac{\partial p}{\partial T} \right)_{V_2} - \frac{1}{2} \Delta p \right) \Delta V \tag{3}$$

where $\Delta p = p_2 - p_1$ is the pressure rise and $\Delta V = V_2 - V_1$ is the change of volume. The pressure derivative is obtained from an equation of state. Precise values for the pressure derivative were required, since this quantity has a significant influence on the adjustment for the change-of-volume work. The first estimates of this derivative were calculated with an extended corresponding states model. Then, the first iteration of the C_v values were fitted to a preliminary equation of state. The derivatives were recalculated with the preliminary equation of state, leading to better C_v values. This calculation required four iterations of fitting until the differences in heat capacity from the previous iteration were less than 0.001%.

A minor adjustment is applied to the number of moles contained in the bomb. The total mass of the sample weighed is corrected by the amount residing in the noxious volume (combined internal volume of pressure transducer, charging valve, and tubing), which is approximately 0.2% of the bomb volume. This amount is calculated from the noxious volume and densities obtained from an equation of state by using a quadratic temperature profile along the length of the capillary and pressure transducer.

Another minor adjustment is applicable only to the two-phase data. The number of moles residing in the noxious volume varies with the temperature and pressure of the sample in the bomb. In this volume, the substance is in the vapor state. Therefore, the raw heat capacity data must be corrected by the energy spent to evaporate the number of moles driven into the noxious volume during the heating interval.

The heat-capacity data of each run are presented in Tables I and II for two-phase states, and in Tables III and IV for single-phase liquid states. For the temperature (ITS-90), the average of the initial and final temperatures of each heating interval is given. In the single-phase liquid region, the tabulated pressures are calculated from pseudo-isochoric fits of the (p, T)-data of each isochore. For each isochore, a seven-term function $p = f(T)$, adopted from the equation of state of Jacobsen and Stewart [8] was fitted to the data. In the two-phase region, however, most of the measured vapor pressures are below the range of high-accuracy readings of the pressure gauge (3 to 70 MPa). For this reason, the pressures were calculated from vapor-pressure equations [9, 10] and are not presented as experimental data in the tables. The density, given in Tables III and IV for single-phase liquid states, is calculated from the corrected number of moles and the bomb volume. In Tables I and II, values of the two-phase heat capacity at constant volume ($C_v^{(2)}$) are presented as well as values of the saturated-liquid heat capacity C_σ (also known as $C'_x = T(dS'/dT)$). Values of C_σ are obtained by adjusting $C_v^{(2)}$ data with the equation given by Rowlinson [11]

$$C_\sigma = C_v^{(2)} - \frac{T}{\rho^2}\frac{d\rho_\sigma}{dT}\frac{dp_\sigma}{dT} + T\left(\frac{1}{\rho_\sigma} - \frac{1}{\rho}\right)\frac{d^2 p_\sigma}{dT^2} \tag{4}$$

where ρ_σ and p_σ are the density and the pressure of the saturated liquid and ρ is the bulk density of the sample residing in the bomb. The derivative quantities were calculated with the ancillary equations of Outcalt and McLinden [9, 10].

The saturated-liquid heat capacity C_σ, as a saturation quantity, depends on a single variable, temperature. If the data are internally consistent,

Table I. Two-Phase Heat Capacity $C_v^{(2)}$ and Heat Capacity of Saturated Liquid C_σ of R152a

T (K)	$\rho_{\sigma,\text{avg}}$ (mol · L^{-1})	$p_{\sigma,\text{avg}}{}^{a,b}$ (MPa)	$C_v^{(2)}$ (J · mol^{-1} · K^{-1})	C_σ (J · mol^{-1} · K^{-1})
162.6371	17.833	0.0002	99.48	99.47
164.8155	17.773	0.0002	99.66	99.65
166.9061	17.715	0.0003	99.77	99.75
169.0700	17.655	0.0004	99.74	99.73
171.1473	17.597	0.0005	100.09	100.07
173.2928	17.537	0.0006	99.98	99.96
175.3744	17.479	0.0007	99.88	99.86
179.5738	17.362	0.0011	100.25	100.22
181.6327	17.304	0.0013	100.62	100.58
183.7548	17.244	0.0016	100.43	100.39
185.7637	17.188	0.0019	100.73	100.68
187.8901	17.128	0.0023	101.10	101.05
189.8629	17.072	0.0027	100.97	100.92
191.9879	17.012	0.0033	101.10	101.04
196.0482	16.896	0.0045	101.43	101.35
200.0957	16.780	0.0061	101.61	101.52
202.0482	16.724	0.0071	101.89	101.79
204.1358	16.664	0.0082	102.07	101.96
206.0734	16.608	0.0094	102.33	102.21
208.1465	16.548	0.0108	102.48	102.35
210.0544	16.492	0.0123	102.54	102.40
212.1332	16.432	0.0141	103.10	102.95
213.9907	16.377	0.0158	102.94	102.77
216.0952	16.316	0.0180	103.36	103.18
217.9074	16.262	0.0201	103.58	103.39
220.0072	16.200	0.0228	103.69	103.49
223.8995	16.084	0.0286	104.26	104.04
225.7149	16.030	0.0317	104.32	104.09
227.7714	15.968	0.0355	104.76	104.52
229.5773	15.914	0.0391	104.99	104.74
231.6096	15.853	0.0436	105.42	105.16
233.3990	15.798	0.0478	105.47	105.19
235.4249	15.736	0.0530	105.92	105.64
237.2013	15.682	0.0579	105.97	105.67
239.2215	15.620	0.0640	106.40	106.10
242.9877	15.503	0.0766	106.82	106.50
250.4687	15.268	0.1074	108.19	107.86
252.2114	15.212	0.1159	108.51	108.18
254.1822	15.149	0.1260	108.75	108.42
255.9141	15.093	0.1355	109.32	108.99
257.8719	15.030	0.1469	109.58	109.25
259.5977	14.974	0.1576	109.83	109.51
261.5485	14.910	0.1704	109.95	109.64

Table I. *(Continued)*

T (K)	$\rho_{\sigma,\text{avg}}$ (mol · L^{-1})	$p_{\sigma,\text{avg}}$ [a,b] (MPa)	$C_v^{(2)}$ (J · mol^{-1} · K^{-1})	C_σ (J · mol^{-1} · K^{-1})
263.2630	14.853	0.1822	110.53	110.22
265.1908	14.789	0.1964	110.65	110.36
268.8353	14.667	0.2254	111.49	111.23
270.5443	14.610	0.2401	111.53	111.30
272.4806	14.544	0.2576	112.16	111.95
276.1095	14.419	0.2931	112.84	112.68
279.7196	14.293	0.3320	113.67	113.59
281.3531	14.235	0.3509	114.28	114.23
283.3177	14.165	0.3747	114.58	114.58
284.9340	14.107	0.3952	114.87	114.92
286.8977	14.036	0.4212	115.14	115.24
288.5131	13.977	0.4435	115.76	115.92
292.0801	13.846	0.4961	116.14	116.43
293.9998	13.774	0.5262	116.88	117.25
297.5080	13.641	0.5850	117.53	118.06
299.1478	13.578	0.6140	118.10	118.71
301.0038	13.506	0.6483	118.72	119.44
302.6614	13.441	0.6800	119.06	119.88
304.4901	13.368	0.7164	119.60	120.53
306.1538	13.301	0.7508	120.20	121.24
311.4236	13.086	0.8679	120.93	122.38
313.0962	13.016	0.9078	121.29	122.89
314.8787	12.940	0.9518	121.94	123.71

[a] Subscript avg denotes a condition evaluated at the average of the initial and final temperatures.
[b] p_σ calculated from Ref. 9.

Table II. Two-Phase Heat Capacity $C_v^{(2)}$ and Heat Capacity of Saturated Liquid C_σ of R143a

T (K)	$\rho_{\sigma,\text{avg}}$ (mol · L^{-1})	$p_{\sigma,\text{avg}}$ [a,b] (MPa)	$C_v^{(2)}$ (J · mol^{-1} · K^{-1})	C_σ (J · mol^{-1} · K^{-1})
164.8070	15.718	0.0015	101.70	101.63
167.0908	15.654	0.0019	102.07	101.99
169.5763	15.585	0.0024	102.30	102.20
171.8324	15.522	0.0030	102.46	102.35
174.2884	15.452	0.0037	102.93	102.80
176.5223	15.389	0.0045	103.09	102.94
178.9530	15.320	0.0055	103.54	103.36

Table II. *(Continued)*

T (K)	$\rho_{\sigma,\text{avg}}$ (mol · L^{-1})	$p_{\sigma,\text{avg}}{}^{a,b}$ (MPa)	$C_v^{(2)}$ (J · mol^{-1} · K^{-1})	C_σ (J · mol^{-1} · K^{-1})
181.1703	15.256	0.0065	103.59	103.39
183.5699	15.187	0.0079	104.16	103.94
185.7765	15.124	0.0093	104.34	104.09
188.1431	15.055	0.0111	104.79	104.51
190.3388	14.991	0.0130	105.12	104.81
192.6723	14.922	0.0153	105.80	105.47
194.8503	14.858	0.0177	105.84	105.47
197.1617	14.789	0.0206	106.36	105.96
199.3215	14.724	0.0237	106.60	106.16
201.6066	14.655	0.0273	106.90	106.42
203.7498	14.591	0.0311	107.34	106.82
206.0062	14.522	0.0356	107.80	107.24
208.1359	14.457	0.0403	108.23	107.64
210.3715	14.388	0.0457	108.55	107.91
212.4839	14.322	0.0513	109.11	108.44
214.6957	14.253	0.0578	109.43	108.71
216.7947	14.187	0.0645	109.77	109.02
218.9846	14.118	0.0722	110.40	109.61
227.4281	13.845	0.1089	112.60	111.65
229.4981	13.777	0.1198	112.74	111.75
231.6137	13.707	0.1319	113.41	112.39
233.6641	13.639	0.1444	113.59	112.53
235.7617	13.569	0.1581	114.39	113.31
237.7949	13.500	0.1724	114.80	113.69
239.8719	13.429	0.1880	115.42	114.29
241.8978	13.359	0.2043	115.80	114.65
243.9577	13.288	0.2219	116.40	115.22
245.9631	13.217	0.2401	117.03	115.84
250.0022	13.074	0.2804	118.19	116.98
252.0213	13.001	0.3024	118.58	117.38
254.0127	12.929	0.3253	118.91	117.72
256.0161	12.856	0.3497	119.71	118.53
257.9869	12.782	0.3751	120.18	119.01
259.9779	12.708	0.4020	120.69	119.56
261.9411	12.634	0.4301	121.12	120.01
263.9041	12.559	0.4596	121.87	120.81
265.8598	12.483	0.4904	122.21	121.20
267.8159	12.406	0.5229	123.17	122.22

Table II. *(Continued)*

T (K)	$\rho_{\sigma,\text{avg}}$ (mol · L^{-1})	$p_{\sigma,\text{avg}}$[a,b] (MPa)	$C_v^{(2)}$ (J · mol^{-1} · K^{-1})	C_σ (J · mol^{-1} · K^{-1})
269.7587	12.330	0.5566	123.43	122.55
273.6242	12.174	0.6287	124.81	124.10
277.4786	12.014	0.7074	126.07	125.59
279.3869	11.934	0.7490	127.05	126.71
281.3024	11.852	0.7925	127.51	127.33
283.1927	11.770	0.8373	128.16	128.14
285.1039	11.686	0.8845	128.95	129.13
286.9835	11.602	0.9329	129.48	129.87
288.8803	11.516	0.9836	130.11	130.73
290.7438	11.430	1.0355	130.95	131.84
294.4922	11.253	1.1459	132.18	133.67
296.3541	11.162	1.2039	132.79	134.62
300.0538	10.977	1.3257	134.69	137.33
301.9145	10.881	1.3903	135.14	138.26
303.7437	10.784	1.4561	135.62	139.25
305.5996	10.684	1.5252	136.88	141.09
307.4036	10.584	1.5947	136.74	141.57
309.2661	10.479	1.6689	137.75	143.31
311.0452	10.375	1.7422	138.64	144.96
304.0523	10.768	1.4674	145.37	139.43
306.2426	10.649	1.5497	146.25	140.66
308.3481	10.531	1.6320	147.57	142.39
312.6122	10.282	1.8088	150.20	146.14
314.7920	10.148	1.9046	152.00	148.68
316.8343	10.018	1.9977	153.09	150.63
325.1497	9.428	2.4137	160.50	163.67
327.2932	9.256	2.5310	163.01	168.59
329.2690	9.087	2.6432	164.40	172.77
331.3935	8.892	2.7681	167.21	179.44
333.3317	8.700	2.8862	169.41	186.25
335.4371	8.471	3.0192	172.68	196.33
337.3469	8.239	3.1442	175.41	207.84
339.4069	7.953	3.2841	180.19	227.08
341.2663	7.646	3.4150	185.13	254.16
343.4200	7.182	3.5729	167.16	292.63

[a] Subscript avg denotes a condition evaluated at the average of the initial and final temperatures.

[b] p_σ calculated from Ref. 10.

Table III. Heat Capacity C_v of Liquid R152a

T (K)	ρ_{avg} (mol · L^{-1})	p_{avg}[a] (MPa)	C_v (J · mol^{-1} · K^{-1})
164.2305	17.896	8.903	68.47
168.3638	17.875	16.441	68.71
172.4621	17.854	23.743	69.08
174.7253	17.843	27.726	68.94
176.5224	17.834	30.870	69.64
186.6279	17.250	5.728	68.15
190.7495	17.231	12.211	68.71
192.5569	17.223	15.031	68.61
194.8352	17.213	18.564	68.88
196.6300	17.204	21.329	68.93
198.8941	17.194	24.791	69.35
200.6744	17.186	27.490	69.28
202.9139	17.176	30.854	69.57
212.0842	16.528	4.924	69.13
214.2033	16.520	7.750	69.17
216.1625	16.512	10.349	69.39
218.2660	16.504	13.122	69.49
222.3026	16.488	18.391	69.77
224.2446	16.481	20.900	70.13
226.3064	16.473	23.544	70.19
228.2340	16.465	25.997	70.64
230.2770	16.457	28.578	70.71
232.2033	16.450	30.993	71.16
239.1601	15.730	4.192	70.31
241.1884	15.723	6.429	70.43
243.2038	15.716	8.641	70.79
247.2244	15.703	13.018	71.35
249.2580	15.696	15.214	71.46
251.2208	15.690	17.322	71.92
253.2553	15.683	19.494	71.98
255.1956	15.677	21.554	72.28
259.1340	15.664	25.697	72.66
261.1626	15.657	27.812	72.85
263.0467	15.651	29.764	73.23
265.0773	15.645	31.854	73.40
262.0871	15.027	4.112	72.20
263.9639	15.022	5.854	72.35
266.1362	15.016	7.865	72.55
267.9869	15.010	9.573	72.73
270.1639	15.004	11.573	72.92
271.9894	14.999	13.244	73.20
274.1650	14.993	15.227	73.34
275.9661	14.988	16.861	73.71
278.1458	14.981	18.830	74.02

Table III. *(Continued)*

T (K)	ρ_{avg} (mol · L^{-1})	p_{avg}[a] (MPa)	C_v (J · mol^{-1} · K^{-1})
282.0988	14.970	22.375	74.32
283.8473	14.965	23.932	74.78
286.0329	14.959	25.869	74.67
287.7488	14.954	27.383	75.23
289.9306	14.948	29.298	75.27
293.8240	14.937	32.691	75.80
288.0405	14.150	3.597	74.52
289.9902	14.145	5.057	75.18
292.0922	14.140	6.628	75.35
294.0453	14.136	8.085	75.49
298.0813	14.126	11.085	75.66
300.1578	14.121	12.623	76.05
302.0982	14.117	14.055	76.33
304.1544	14.112	15.567	76.60
308.1387	14.103	18.484	77.15
312.1127	14.093	21.372	77.43
316.0694	14.084	24.227	78.00
320.0177	14.075	27.057	78.59
323.9573	14.066	29.860	78.95
327.8836	14.057	32.637	79.22
329.8431	14.052	34.016	79.43
306.1876	13.468	3.260	76.64
308.2253	13.464	4.549	76.91
310.3180	13.459	5.872	77.22
312.3627	13.455	7.162	77.37
316.4948	13.447	9.764	77.71
318.5128	13.443	11.031	77.70
322.5989	13.435	13.589	78.35
326.6732	13.426	16.129	78.68
328.8479	13.422	17.480	79.13
332.9423	13.414	20.014	79.64
337.0356	13.405	22.534	80.15
338.8581	13.402	23.651	80.21
341.1235	13.397	25.035	80.39
342.9291	13.393	26.136	80.51
327.1226	12.571	3.027	79.29
331.3742	12.564	5.171	79.66
333.5828	12.560	6.285	79.80
335.6247	12.557	7.314	79.92
339.8725	12.549	9.454	80.28
342.1118	12.546	10.581	80.71

[a] Subscript avg denotes a condition evaluated at the average of the initial and final temperatures.

Table IV. Heat Capacity C_v of Liquid R143a

T (K)	ρ_{avg} (mol · L^{-1})	p_{avg}[a] (MPa)	C_v (J · mol^{-1} · K^{-1})
172.5565	15.644	7.938	68.43
175.2451	15.633	11.952	68.59
177.0298	15.626	14.628	68.71
179.6599	15.616	18.561	69.13
181.4563	15.609	21.229	69.26
184.0426	15.599	25.031	69.51
185.8380	15.592	27.642	69.74
187.8542	15.584	30.546	70.27
188.3914	15.582	31.315	70.16
190.7988	15.127	7.302	69.64
192.8861	15.120	10.014	69.78
195.1668	15.112	13.029	70.35
197.2441	15.105	15.773	70.21
199.5162	15.097	18.738	70.81
201.5735	15.090	21.378	70.79
203.8414	15.082	24.239	71.25
205.8816	15.075	26.779	71.50
208.1183	15.067	29.549	71.87
210.1512	15.061	32.078	72.33
208.0073	14.621	6.483	71.10
210.2338	14.614	8.993	71.48
212.3681	14.607	11.432	71.57
214.5824	14.601	13.967	71.97
216.6730	14.594	16.344	72.24
218.8695	14.587	18.817	72.46
220.9379	14.581	21.118	72.75
223.1052	14.574	23.504	73.18
225.1740	14.568	25.760	73.55
227.3037	14.562	28.068	73.71
231.4567	14.549	32.556	74.21
227.1426	14.029	5.662	73.08
229.4664	14.023	7.848	73.47
231.4525	14.017	9.748	73.55
233.7754	14.011	11.994	73.92
235.7224	14.006	13.884	74.21
238.0428	13.999	16.134	74.65
239.9519	13.994	17.974	74.92
242.2762	13.988	20.192	75.33
244.1186	13.983	21.929	75.40
246.4717	13.977	24.120	75.95
248.2543	13.972	25.761	76.31
250.6216	13.966	27.923	76.38
252.3632	13.961	29.508	76.86
254.7225	13.955	31.662	76.91
256.4376	13.951	33.248	77.28
246.3316	13.416	5.297	75.70
248.5641	13.411	7.109	75.70

Table IV. *(Continued)*

T (K)	ρ_{avg} (mol · L^{-1})	p_{avg}[a] (MPa)	C_v (J · mol^{-1} · K^{-1})
250.6151	13.406	8.790	75.93
252.8096	13.401	10.594	76.45
257.0440	13.391	14.055	77.15
259.0325	13.386	15.665	77.23
261.2524	13.381	17.450	77.55
263.2223	13.377	19.025	77.90
265.4046	13.372	20.760	78.21
267.3757	13.367	22.321	78.53
269.5373	13.362	24.028	78.55
271.5082	13.358	25.579	78.88
273.6539	13.353	27.265	79.03
275.6050	13.348	28.793	79.43
277.7473	13.344	30.464	80.04
279.6657	13.339	31.952	80.36
281.8059	13.334	33.599	80.68
266.3008	12.723	4.962	78.30
270.5437	12.714	7.800	78.87
272.6139	12.710	9.189	78.95
274.7462	12.706	10.622	79.05
276.8307	12.702	12.023	79.60
278.9228	12.698	13.430	79.68
281.0129	12.694	14.833	80.28
283.0800	12.690	16.218	80.43
285.1712	12.685	17.615	80.74
287.2151	12.681	18.974	81.02
289.3142	12.677	20.364	81.34
291.3260	12.673	21.689	81.75
293.4552	12.669	23.085	81.87
295.4210	12.665	24.367	82.22
299.4935	12.658	27.004	82.66
301.6745	12.653	28.408	83.13
303.5678	12.650	29.625	83.43
305.7566	12.645	31.031	83.95
307.6398	12.642	32.242	84.11
309.8085	12.637	33.642	84.45
285.4336	11.952	4.171	81.15
289.7480	11.945	6.525	81.47
291.8811	11.942	7.688	81.58
294.0396	11.938	8.863	81.79
296.1097	11.935	9.989	82.23
298.2870	11.931	11.172	82.43
300.3274	11.928	12.279	83.05
304.5601	11.921	14.569	83.50
306.7747	11.917	15.764	83.85
308.7748	11.914	16.841	83.71
310.9964	11.910	18.035	84.02
312.9743	11.907	19.095	84.29

Table IV. *(Continued)*

T (K)	ρ_{avg} (mol · L^{-1})	p_{avg}[a] (MPa)	C_v (J · mol^{-1} · K^{-1})
315.1688	11.904	20.269	84.77
317.1429	11.901	21.323	84.80
319.3687	11.897	22.508	85.36
321.2830	11.894	23.525	85.38
323.5440	11.890	24.724	85.73
325.4079	11.887	25.709	86.11
327.6870	11.883	26.911	86.60
329.5205	11.880	27.876	86.64
331.8295	11.876	29.088	87.20
333.6453	11.874	30.038	87.12
335.9567	11.870	31.246	87.46
337.7613	11.867	32.186	87.35
340.0821	11.863	33.392	87.69
341.8592	11.860	34.313	88.20
302.6082	11.081	3.135	83.69
304.9506	11.078	4.132	83.74
306.9944	11.075	4.999	83.97
309.3185	11.072	5.986	83.93
313.6729	11.066	7.837	84.82
318.0323	11.061	9.696	85.16
322.3770	11.055	11.551	85.43
326.7105	11.049	13.398	86.02
328.8573	11.046	14.311	86.43
333.1596	11.041	16.136	86.73
335.3561	11.038	17.065	86.81
337.4661	11.035	17.957	87.18
339.6743	11.032	18.891	87.50
341.7628	11.029	19.775	87.62
322.6664	10.000	3.728	87.22
323.8406	9.999	4.091	87.21
326.2608	9.996	4.843	87.39
328.3871	9.994	5.505	87.61
329.5622	9.993	5.872	87.75
330.8087	9.992	6.262	87.92
331.7354	9.991	6.552	87.99
332.9560	9.989	6.935	88.07
334.1053	9.988	7.295	87.97
335.3547	9.987	7.688	88.10
336.2793	9.986	7.979	88.29
338.6302	9.984	8.719	88.22
339.8803	9.982	9.113	88.46
342.0863	9.980	9.809	88.63

[a] Subscript avg denotes a condition evaluated at the average of the initial and final temperatures.

then the values at saturation from different isochores should fall on a single curve. Though the C_σ values were evaluated from experiments with different amounts of sample in the calorimeter, the results should demonstrate consistency of all isochores. The saturated liquid heat capacities for all of the filling densities are depicted graphically in Figs. 1 and 2. In order to intercompare the data from different isochores, an equation which accurately describes the whole two-phase data set was derived for each fluid.

For R152a, the two-parameter expression,

$$C_\sigma/C_0 = a_1 + a_2 T_r^{17/4} \tag{5}$$

where $C_0 = 1\ \text{J} \cdot \text{mol}^{-1} \cdot \text{K}^{-1}$, $T_r = T/T_c$, $T_c = 386.411$ K, $a_1 = 97.954777$, and $a_2 = 61.714966$ was fitted by applying software based on the Wagner method of structural optimization [12]. Equation (5) is valid at temperatures from 163 to 314 K. For R143a, the five-parameter expression,

$$\ln(C_\sigma/C_0) = b_1 + b_2 T_r^{-2} + b_3 T_r^{-3/4} + b_4 T_r^{1/2} + b_5 T_r^{21/4} \tag{6}$$

where $C_0 = 1\ \text{J} \cdot \text{mol}^{-1} \cdot \text{K}^{-1}$, $T_r = T/T_c$, $T_c = 346.04$ K, $b_1 = 2.85154624 \times 10^{-2}$, $b_2 = -2.30892154 \times 10^{-5}$, $b_3 = 5.0265572$, $b_4 = -0.64777439$, and $b_5 = 0.53608423$ was fitted by applying the same method. Equation (6) is

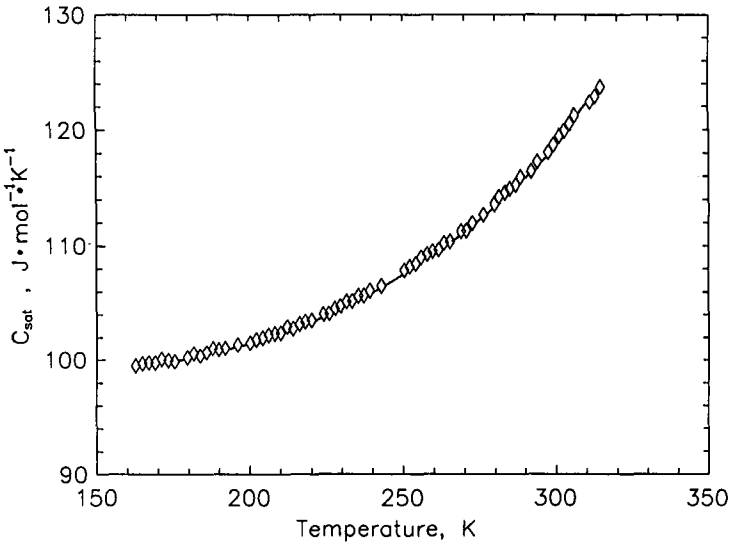

Fig. 1. Experimental saturated-liquid heat capacity (C_σ) values for R152a.

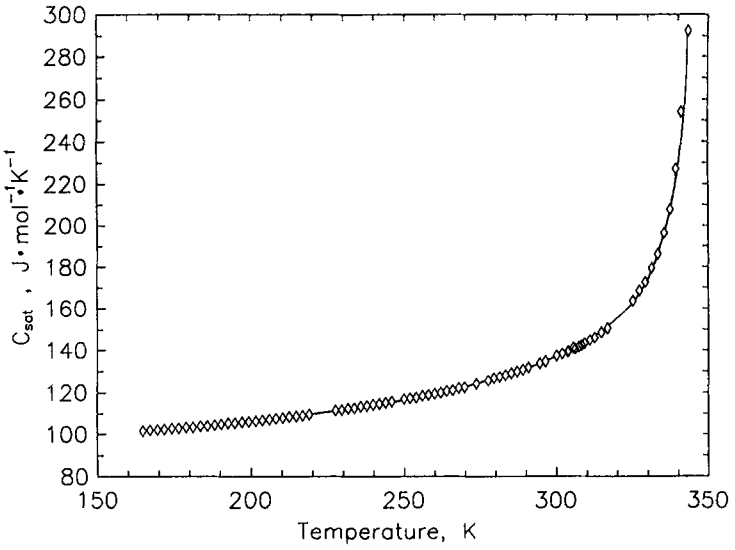

Fig. 2. Experimental saturated-liquid heat capacity (C_σ) values for R143a.

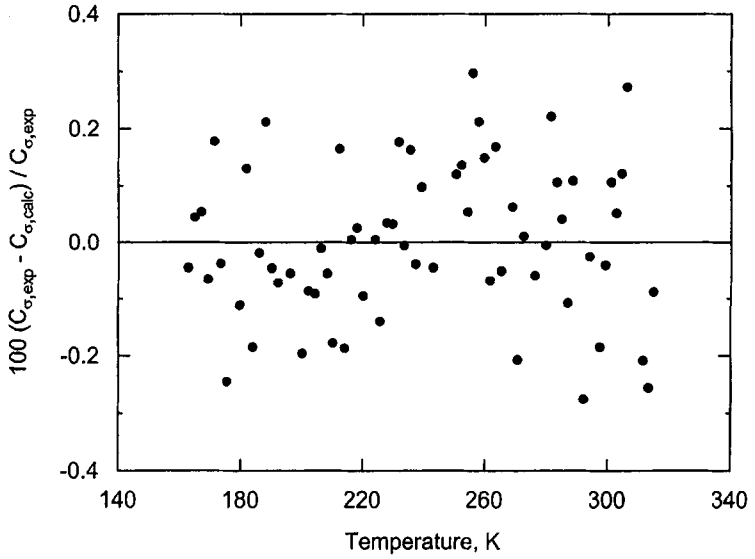

Fig. 3. Comparison of experimental C_σ results for R152a with the values calculated with Eq. (5).

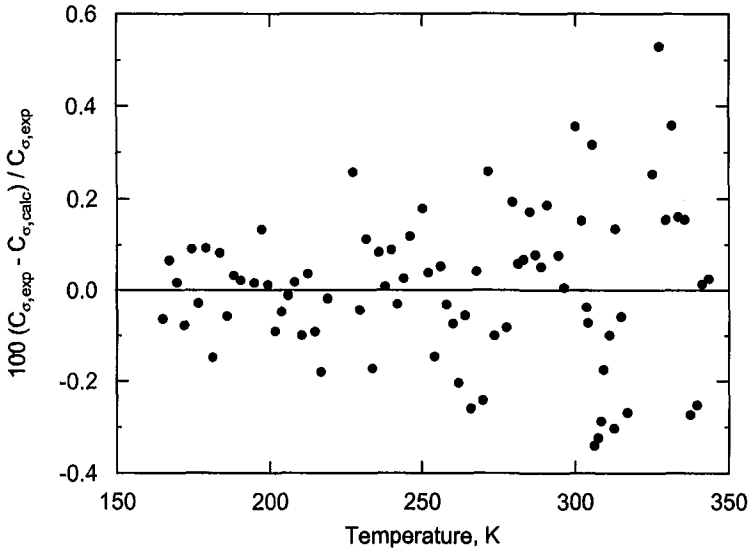

Fig. 4. Comparison of experimental C_σ results for R143a with the values calculated with Eq. (6).

valid at temperatures from 165 to 343 K. The deviations are shown in Figs. 3 and 4. Deviations are distributed randomly over the entire temperature range; the standard deviation of the fit was found to be 0.15 $J \cdot mol^{-1} \cdot K^{-1}$ for R152a and 0.25 $J \cdot mol^{-1} \cdot K^{-1}$ for R143a. The heat capacities at saturation from different isochores agree within the uncertainty of the measurements, indicating that there is good internal consistency within each data set.

Values of the single-phase liquid heat capacity are shown in Figs. 5 and 6. The data are presented on isochores in a C_v-T diagram. Most isochores overlap in their temperature ranges. Figure 6 shows that for R143a, the slope of each C_v-T isochore is nearly independent of the density of the isochore. Except for the lowest density isochore which shows a small critical enhancement, almost all of the R143a data fall on a single line. Conversely, the R152a data in Fig. 5 show about the same slope of each C_v-T isochore, but the intercept increases as density increases. For this reason, the high density liquid C_v data for R152a have higher than expected values for this group of substances.

When this document was prepared, the only other published heat capacity data for R152a and R143a were the four sets of isobaric heat capacity (C_p) data mentioned earlier. Though most of the published data

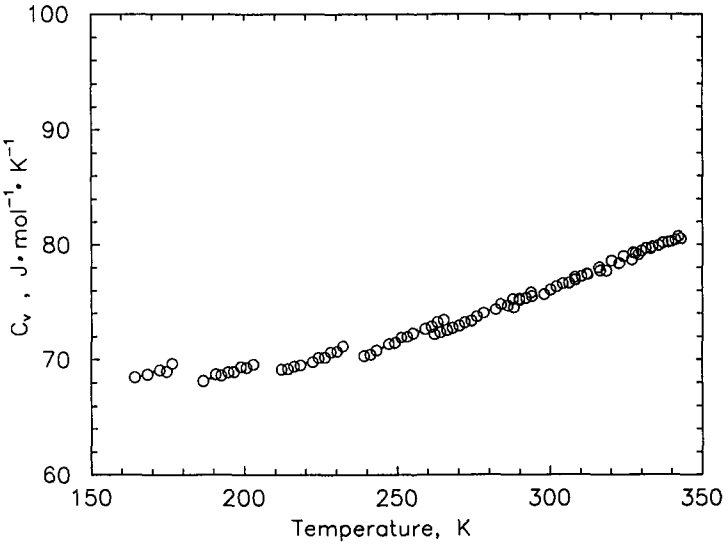

Fig. 5. Experimental liquid-phase heat capacity (C_v) data for R152a.

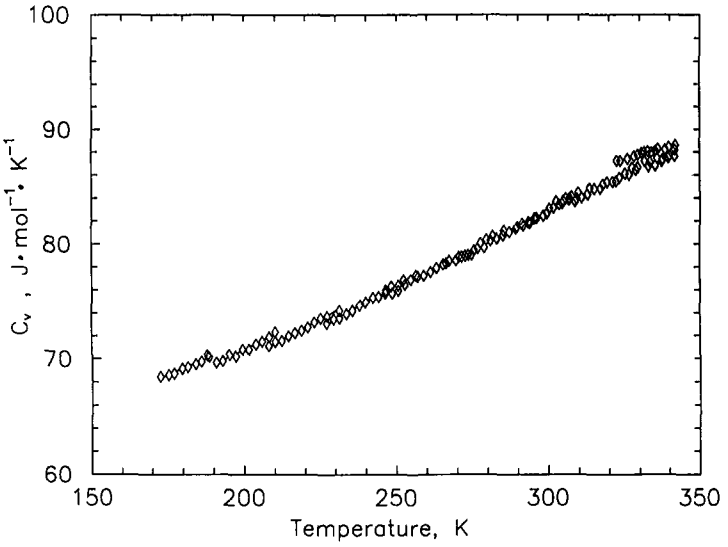

Fig. 6. Experimental liquid-phase heat capacity (C_v) data for R143a.

are of high accuracy, those values were not used in the development of the equations of state of Outcalt and McLinden [9, 10]. Since the present results were used by Outcalt and McLinden, their equations of state will facilitate an indirect comparison with published data. Figures 7 and 8 in Ref. 9 show comparisons of C_v and C_p, respectively, with the equation of state of Outcalt and McLinden for R152a. The absolute average deviation (AAD) for the C_v data from this work is 0.79% with a bias of +0.76%. The AAD for the C_p data of Kubota et al. [3] is 6.84% with a bias of +6.84%. The AAD for the C_p data of Nakagawa et al. [4] is 1.20% with a bias of −1.20%. The AAD for the C_p data of Porichanski et al. [5] is 2.31% with a bias of +0.06%. Except for Kubota et al., this work is in very good agreement with published heat capacities for R152a. There is, however, a 65 K gap between 155 and 220 K, where no published data exist for comparison with this study of R152a.

Figures 8 and 9 in Ref. 10 show comparisons of C_v and C_p with the equations of state of Outcalt and McLinden for R143a. The AAD for the C_v data from this work is 0.46% with a bias of +0.17% and for the C_σ data the AAD is 0.14% with a bias of −0.14%. The AAD for the saturated-liquid C_p data of Russell et al. [6] is 0.26% with a bias of −0.17%; the agreement with the present C_σ is excellent. Taken as a whole, most of the calculated values of C_v are within ±1% of the measurements and most of the C_p values are within ±2%.

3.2. Derived Vapor Pressures

Vapor pressures measured between the triple point and the normal boiling point with traditional techniques are often inaccurate. In some cases, volatile impurities concentrate in the vapor phase [13]. This will influence the vapor pressure measurement, making it appear larger than the true value for the pure substance. In other instances, the pressure gauges are not accurate enough at these low pressure conditions. This situation can be remedied to some extent, however, by extracting vapor pressure values from saturated-liquid heat capacity measurements. These C_σ values have a high internal consistency and can be accurate below the normal boiling point because the adjustments to the $C_v^{(2)}$ measurements are less than 2% of the resulting C_σ value. We extracted vapor pressures from the data in Tables I and II by applying a method discussed by Weber [13]. Temperatures (ITS-90) and calculated vapor pressures are presented in Table V for R152a and in Table VI for R143a. Because the method employed by Weber requires a knowledge of the density of the saturated vapor and its first temperature derivative, the expanded uncertainty of the derived vapor pressures is estimated to be 0.05 kPa.

Table V. Vapor Pressures of R152a Derived from C_σ Measurements

T (K)	p_σ (kPa)
170	0.415
180	1.142
190	2.776
200	6.086
210	12.229
220	22.826
230	40.005
240	66.427
250	105.278

3.3. Triple Points

The triple-point temperature (ITS-90) of R152a was measured on three different samples. For these experiments, the sample was slowly cooled to a temperature about 2 K below freezing. Then the solidified sample was heated at a constant power of 0.09 W. In order to obtain a slowly increasing temperature, heater power was set to a value which is less than one-tenth of the power for heat capacity experiments. Data were evaluated graphically. The triple point was located by noting a sharp break in the rate of temperature rise, delineating when melting began. Figure 7 shows the

Table VI. Vapor Pressures of R143a Derived from C_σ Measurements

T (K)	p_σ (kPa)
165	1.560
170	2.511
175	3.915
180	5.931
185	8.755
190	12.617
195	17.790
200	24.588
205	33.365
210	44.520
215	58.488
220	75.748
225	96.816

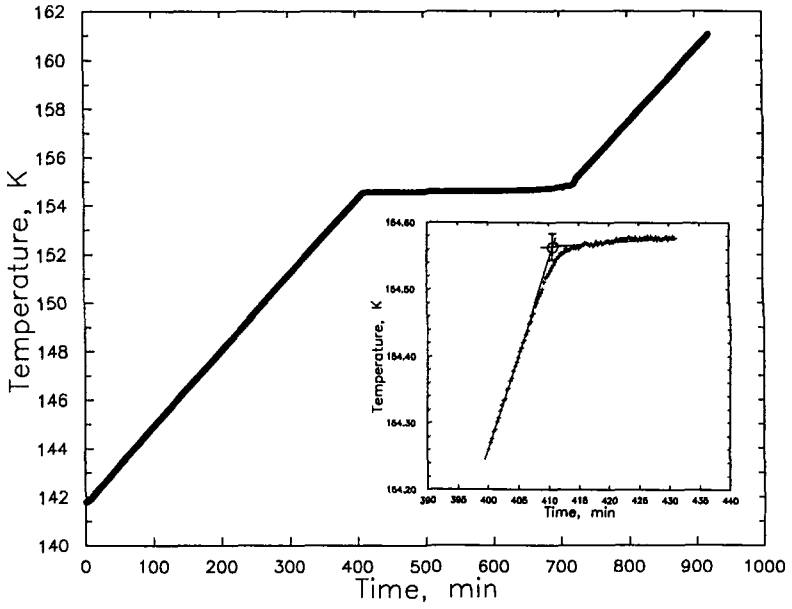

Fig. 7. Temperature–time trace for a triple-point temperature determination for R152a.

temperature-time trace for one such experiment of 15 hours duration. The inset figure shows a magnification of the onset of melting, in a 30 minute time frame, from which the temperature of the triple point was determined by finding the intersection of two lines, through the rising portion and through the plateau portion. The results and their expanded uncertainties for T_{tr} of the three samples were 154.56 ± 0.01 K, 154.57 ± 0.01 K, and 154.56 ± 0.01 K. Thus, the average of 154.56 ± 0.02 K was adopted for T_{tr} of R152a. This agrees exactly with the triple-point temperature measured by Blanke and Weiß [14] of 154.56 ± 0.005 K. The enthalpy of fusion $\Delta_{fus}H$ was measured by integrating the applied heater power over the time of heating and applying a correction for parasitic heat losses. Results and their expanded uncertainties for $\Delta_{fus}H$ obtained from the three runs were 1587 ± 20 J·mol^{-1}, 1560 ± 20 J·mol^{-1}, and 1552 ± 20 J·mol^{-1}; the average of 1566 ± 20 J·mol^{-1} is the best estimate for $\Delta_{fus}H$ at the triple point.

The triple-point temperature of R143a was measured on two different samples. A similar method was used. The power to the bomb heater was 0.09 W. The results and their expanded uncertainties for T_{tr} of the two samples were 161.32 ± 0.02 K and 161.36 ± 0.02 K. As a result, the average of 161.34 ± 0.03 K was adopted for T_{tr} of R143a. An earlier result of Russell

et al. [6], 161.82 ± 0.04 K, is in poor agreement with this study. The exact reasons for this 0.48 K discrepancy are unknown. However, one could explain this discrepancy if the previous study identified the temperature of the sample container after all the solid had melted. In this type of experiment, the elapsed time to melt the solid is typically on the order of 10 hours and may be longer. During the heating interval, the imperfect heat transfer between the container and the sample results in heating the container beyond the true T_{tr}. In this study, about 900 minutes (15 hours) elapsed before the whole sample had melted at which the observed temperature had risen to 161.9 ± 0.1 K. This temperature is 0.56 K above the temperature which was identified as T_{tr}. The results and their expanded uncertainties for $\Delta_{fus}H$ obtained from the two runs were 5823 ± 70 $J \cdot mol^{-1}$ and 5883 ± 70 $J \cdot mol^{-1}$; the average of 5853 ± 70 $J \cdot mol^{-1}$ is the best estimate for $\Delta_{fus}H$ at the triple point. In the course of this work, it was noted that R143a also undergoes a solid-solid transition at 156.57 ± 0.03 K with a heat of transition of 248 ± 20 $J \cdot mol^{-1}$.

3.4. Assessment of Uncertainties

Uncertainty in C_v arises from several sources. Primarily, the accuracy of this method is limited by the uncertainty of the temperature rise measurement and the change-of-volume work adjustment. In the following discussion, the definition for the expanded uncertainty which is two times the standard uncertainty corresponds to a coverage factor $k = 2$ and thus a two-standard-deviation estimate.

Different sources of uncertainty, including calibration of the platinum resistance thermometer, radiation to or from the thermometer head, and drift of the ice point resistance, contribute to an expanded uncertainty of 0.01 K at 100 K to 0.03 K at 345 K for the absolute temperature measurement. Uncertainty of the temperature rise, however, also depends on the reproducibility of temperature measurements. The temperatures assigned to the beginning (T_1) and to the end (T_2) of a heating interval are determined by extrapolation of a linear temperature drift (approximately -1×10^{-3} to 0.5×10^{-3} $K \cdot min^{-1}$) to the midpoint time of the interval. This procedure leads to an uncertainty of 0.001 to 0.004 K for the extrapolated temperatures T_1 and T_2, depending on the standard deviation of the linear function correlated. In all cases, values from 0.002 to 0.006 K were obtained for the uncertainty of the temperature rise, $\Delta T = T_2 - T_1$. For a typical experimental value of $\Delta T = 4$ K, this corresponds to a relative uncertainty of between 0.05 and 0.15%.

The uncertainty of the change-of-volume work influences primarily the single-phase values, since two-phase experiments are performed over a

small pressure interval. For R152a, the ratio of change-of-volume work to total applied heat may be as large as 0.045 for the highest density isochore down to 0.01 for the lowest density. For R143a this range is smaller, 0.005 to 0.033. Estimated uncertainties of 2.3 to 3.0% in the change-of-volume work are due to both the deviation of the calculated pressure derivatives and the uncertainty of the volume change. This leads to a relative uncertainty of 0.2% in C_v for the lowest density isochore up to 0.3% for the highest density.

The energy applied to the calorimeter is the integral of the product of voltage and current from the initial to the final heating time. Voltage and current are measured twenty times during a heating interval. The measurements of the electrical quantities have a relative uncertainty of 0.01%. However, we must account for the effect of radiation heat losses or gains which occur when a time-dependent lag of the controller leads to a small temperature difference of about 20 mK between bomb and radiation shield at the beginning and end of a heating period. Since heat transfer by radiation is proportional to $T_1^4 - T_2^4 \approx 4T^3 \Delta T$ we would expect radiation losses to substantially increase with the bomb temperature. Therefore, the relative uncertainty in the applied heat is estimated to be 0.02% for lower temperatures and up to 0.10% for the highest temperatures. This leads to a relative uncertainty in C_v between 0.04 and 0.20%.

The energy applied to the empty calorimeter has been measured in repeated experiments and fitted to a function of temperature [2]; its relative uncertainty is less than 0.02%. Its influence on the uncertainty of the heat capacity is reduced, because the ratio of the heat applied to the empty calorimeter to the total heat varies only from 0.41 to 0.57 for the single-phase runs and from 0.43 to 0.48 for the two-phase runs. The mass of each sample was determined with a relative uncertainty of 0.01% by differential weighings before and after trapping the sample. The density calculated from this mass and the bomb volume has a relative uncertainty of approximately 0.2%. For pressures, the uncertainty of the gauge of 7 kPa is added to the cross term for the pressure derivative in the change-of-volume work adjustment. However, neither the uncertainty of p nor ρ contributes appreciably to the combined uncertainty for molar heat capacity. We may combine the various sources of experimental uncertainty using a root-sum-of-squares formula. I estimate the relative uncertainty of C_v to be 0.7%; for $C_v^{(2)}$ it is 0.5%, and for C_σ it is 0.7%.

4. CONCLUSIONS

For 1,1-difluoroethane (R152a), a total of 85 liquid-phase heat capacites, 66 saturated liquid heat capacities, 9 derived vapor pressures,

and values for the temperature and enthalpy of fusion at the triple point were reported. For 1,1,1-trifluoroethane (R143a), 136 liquid-phase heat capacities, 80 saturated-liquid heat capacities, 12 derived vapor pressures, and values for the temperature and enthalpy of fusion at the triple point were reported. For R152a, agreement with a published value of the triple-point temperature was within 0.01 K. For R143a, poor agreement was found with a published triple-point temperature. Published liquid-phase heat capacity data for both R152a and R143a are scarce and cover limited ranges of temperature and pressure. Agreement with published liquid-phase heat capacity values at constant pressure was within 2% for R152a for two of the three sources, and was within 1% for R143a.

ACKNOWLEDGMENTS

I am grateful to Mark McLinden and Stephanie Outcalt for generous technical assistance and helpful discussions during this study. I have profitted from many discussions with Torsten Lüddecke, W. M. Haynes, Marcia Huber, and Lloyd Weber. This research project was supported by a grant from the U.S. Department of Energy, Office of Building Technology through the Air-Conditioning and Refrigeration Technology Institute (Grant No. DE-FG02-91CE23810: Materials Compatibilities and Lubricants Research on CFC-Refrigerant Substitutes).

REFERENCES

1. R. D. Goodwin, *J. Res. Natl. Bur. Stand. (U.S.)* **65C**:231 (1961).
2. J. W. Magee, *J. Res. Natl. Inst. Stand. Technol.* **96**:725 (1991).
3. Y. Kubota, H. Sugitani, Y. Tanaka, and T. Makita, *Chemistry Express* **2**:397 (1987).
4. S. Nakagawa, T. Hori, H. Sato, and K. Watanabe, *J. Chem. Eng. Data* **38**:70 (1993).
5. E. G. Porichanski, O. P. Ponomareva, and P. I. Svetlichny, *Izv. Vyssh. Uchebn. Zaved Energ.* **3**:122 (1982) (in Russian).
6. H. Russell, D. R. V. Golding, and D. M. Yost, *J. Am. Chem. Soc.* **66**:16 (1944).
7. R. D. Goodwin and L. A. Weber, *J. Res. Natl. Bur. Stand. (U.S.)* **73A**:1 (1969).
8. R. T Jacobsen and R. B. Stewart, *J. Phys. Chem. Ref. Data* **2**:757 (1973).
9. S. L. Outcalt and M. O. McLinden, *J. Phys. Chem. Ref. Data* **25**:605 (1996).
10. S. L. Outcalt and M. O. McLinden, *Int. J. Thermophys.* **18**:1445 (1997).
11. J. S. Rowlinson, *Liquids and Liquid Mixtures* (Butterworths, London, 1969), p. 37.
12. W. Wagner, *Eine mathematisch statistische Methode zum Aufstellen thermodynamischer Gleichungen—gezeigt am Beispiel der Dampfdruckgleichung reiner Fluide*; Habilitationsschrift TU Braunschweig, FortschrBer VDI-Zeitschriften Reihe 3, Nr.39 (VDI, Düsseldorf, 1974).
13. L. A. Weber, *Int. J. Refrig.* **17**:117 (1992).
14. W. Blanke and R. Weiß, *Fluid Phase Equil.* **80**:179 (1992).